Inorganic Chemistry

Article

pubs.acs.org/IC

Interplay of Strongly Anisotropic Metal Ions in Magnetic Blocking of Complexes

Liviu Ungur,[†] Maarten Thewissen,[†] Jean-Pierre Costes,[‡,§] Wolfgang Wernsdorfer,[⊥] and Liviu F. Chibotaru*[,†]

[†]Afdeling Kwantumchemie en Fysicochemie, Katholieke Universiteit Leuven, Celestijnenlaan 200F B-3001 Heverlee, Belgium
[‡]LCC (Laboratoire de Chimie de Coordination), CNRS, 205 route de Narbonne, BP 44099, F-31077 Toulouse Cedex 4, France
[§]Université de Toulouse, UPS, INPT, F-31077 Toulouse Cedex 4, France
[⊥]Institut Néel, CNRS and Université J. Fourier, BP 166, 38042 Grenoble Cedex 9, France

Supporting Information

A challenging problem: why CoGdCo is a better Single-Molecule Magnet than Dy and Tb analogues?

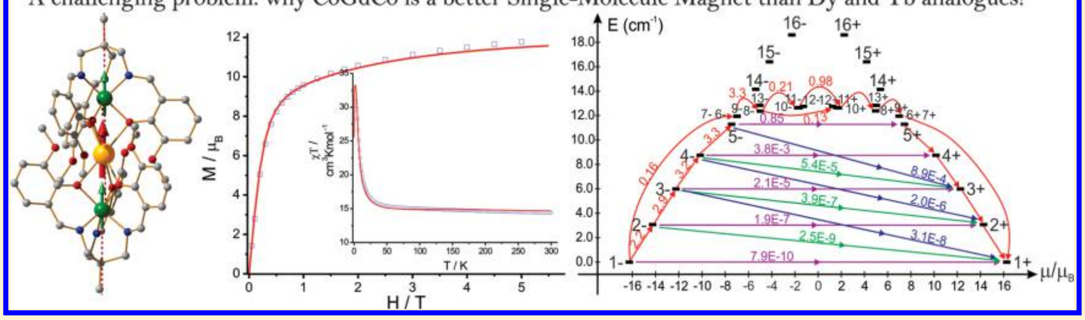

ABSTRACT: The key characteristic of single-molecule magnets (SMMs) is the anisotropy-induced blocking barrier, which should be as efficient as possible, i.e., to be able to provide long magnetic relaxation times at elevated temperatures. The strategy for the design of efficient SMMs on the basis of transition-metal complexes such as $Mn_{12}Ac$ is well established, which is not the case of complexes involving strongly anisotropic metal ions such as cobalt(II) and lanthanides (Ln). While strong intraionic anisotropy in the latter allows them to block the magnetization already in mononuclear complexes, the presence of several such ions in a complex does not result automatically in more efficient SMMs. Here, the magnetic blocking in the series of isostructural 3d−4f complexes $Co^{II}-Ln^{III}-Co^{II}$, Ln = Gd, Tb, and Dy, is analyzed using an originally developed ab initio based approach for the investigation of blocking barriers. The theoretical analysis allows one to explain the counterintuitive result that the Co−Gd−Co complex is a better SMM than terbium and dysprosium analogues. It turns out that the highly efficient magnetic blockage in the Co−Gd−Co complex results from a concomitant effect of unexpectedly large unquenched orbital momentum on Co^{II} ions (ca. 1.7 μB) and the large spin on the gadolinium ($S = {}^{7}/_{2}$), which provides a multilevel blocking barrier, similar to the one of the classical $Mn_{12}Ac$. We conclude that efficient SMMs could be obtained in complexes combining strongly anisotropic and isotropic metal ions with large angular momentum rather than in polynuclear compounds involving strongly anisotropic ions only.

■ INTRODUCTION

Single-molecule magnets (SMMs) are metal complexes showing blockage of magnetization at low temperatures, much as ordinary ferro- and ferrimagnets and regarded for that as potential memory elements in future information storage devices and quantum information processing.[1−6] The first investigated SMMs, $Mn_{12}ac$[1] and Fe_8[2], were complexes corresponding to the so-called strong exchange limit,[7] in which the spread of the exchange levels arising from magnetic interaction between metal ions much exceeds the zero-field splitting on each of them (intraionic anisotropy). In such systems, the exchange multiplets are characterized by the total spin S of the complex, split by anisotropic interactions into $2S + 1$ components. The latter group is split into Kramers doublets for half-integer S and degenerate Ising doublets for integer S in complexes with axial symmetry, with the components $|S,M\rangle$ and $|S,-M\rangle$, where M is the spin projection on the anisotropy axis.[2] The total splitting of the exchange multiplet S due to axial anisotropy only is given by the formula $U_{eff} = DS^2$. In the case of a negative anisotropy constant, $D < 0$, the ground-state doublet corresponds to $M = \pm S$, i.e., to a maximally magnetized state, while the reorientation of magnetization from S to $-S$ occurs via consecutive transitions between $|S,M\rangle$ states for neighboring M values, which correspond to climbing over the barrier U_{eff}.[2] The height of the latter scales with the strength of intraionic anisotropy on the metal ions[2,7] (it usually provides the dominant contribution[8]), while its dependence on the total

Received: November 23, 2012
Published: May 21, 2013

spin is implicitly rather complex because of the spin dependence of the anisotropy constant D.[9−11] However, the larger the ground-state spin, the more steps (i.e., higher orders of the perturbation theory) that are needed to couple states with opposite magnetization (e.g. $|S,+S\rangle$ and $|S,-S\rangle$), leading to a slower relaxation mechanism.[2−12]

The quest for higher magnetization barriers turned the attention of researchers toward strongly anisotropic metal ions, with typical examples being lanthanides.[13−16] The first synthesized pure Ln SMMs were mononuclear double-decker complex $[\mathrm{Ln(Pc)_2}]^-$ (Pc = dianion of phthalocyanine),[14] among which the Ln = Tb compound has shown a very high blocking barrier, U = 260 cm^{-1}, and a relaxation time on the order of seconds for temperatures of around 1 K. Such a remarkable SMM behavior is entirely due to the high symmetry of the complex, close to D_{4d}, which is the reason for the strong suppression of quantum tunneling of magnetization (QTM). Note that for an ideal D_{4d} symmetry QTM in $[\mathrm{Tb(Pc)_2}]^-$ would be completely suppressed.[17] Accordingly, in mononuclear lanthanide complexes based on polyoxometalates,[15] $[\mathrm{Ln(W_5O_{18})_2}]^{9-}$ and $[\mathrm{Ln(\beta_2\text{-}SiW_{11}O_{39})_2}]^{13-}$, showing a stronger departure from an ideal D_{4d} symmetry, the SMM behavior is less pronounced. A more robust SMM behavior, not sensitive to the site symmetry, is generally expected in polynuclear complexes. However, the magnetic blocking in exchange-coupled compounds with strongly anisotropic metal ions is more involved because it represents a superposition of exchange and intraionic mechanisms.[18] The investigations have shown[18−21] that despite the high activation barriers of individual metal ions the magnetic blocking is generally not more efficient than that in mononuclear lanthanide complexes for temperatures on the order of exchange splitting, which is not very large in pure lanthanide complexes. Exceptions are the $\mathrm{N_2}^{3-}$ radical-bridged lanthanide complexes, where the exchange interaction is larger than in pure lanthanide complexes by 2 orders of magnitude.[22,23]

The direct way to enhance the exchange interaction is by designing mixed lanthanide−transition metal complexes.[24−26] Intuitively, one may think that all metal ions in such mixed complexes should be strongly anisotropic in order to achieve the highest SMM efficiency. This, however, turned out not to be the case, as was found for recently investigated complexes $\mathrm{Co^{II}{-}Ln^{III}{-}Co^{II}}$, where Ln = lanthanide.[27] This isostructural series is best suited for investigation of the interplay of strongly anisotropic metal ions in the mixed SMMs and will be considered further in this article. Note that other series of linear trimetallic compounds with the $\mathrm{Co^{II}{-}Ln^{III}{-}Co^{II}}$ core have exhibited similar SMM behavior,[28,29] so that the results of the present analysis are expected to apply for these compounds also.

■ A CHALLENGING PROBLEM: WHY IS $\mathrm{CO^{II}{-}GD^{III}{-}CO^{II}}$ A BETTER SMM THAN $\mathrm{CO^{II}{-}TB^{III}{-}CO^{II}}$ AND $\mathrm{CO^{II}{-}DY^{III}{-}CO^{II}}$?

For the present theoretical analysis, we have chosen three complexes, $\mathrm{Co^{II}{-}Ln^{III}{-}Co^{II}}$ with Ln = Gd (**1**), Tb (**2**), and Dy (**3**).[27] They were prepared by using a tripodal nonadentate Schiff base ligand, *N*,*N*′,*N*″-tris(2-hydroxy-3-methoxybenzilidene)-2-(aminomethyl)-2-methyl-1,3-propanediamine. The synthesis, characterization, and magnetic properties of these compounds have been previously described.[27] The structure of **1** is shown in Figure 1 (see Figures S1 and S2 in the Supporting Information for the structures of **2** and **3**, respectively). Despite the lack of strict symmetry in these complexes, their structures can be approximately described as trigonal, with the three metal ions lying on a common axis (Figure 1b) and having roughly equivalent Co sites. The compounds **1** and **2** crystallize in the centrosymmetric $C2/c$ space group with Z = 12, while **3** crystallizes in the chiral $P2_12_12_1$ space group with Z = 4.[27]

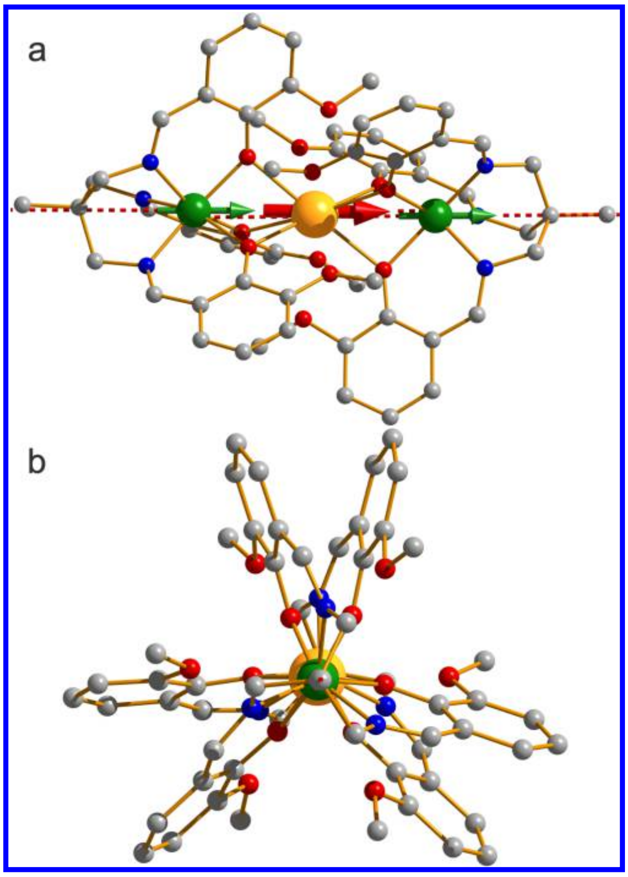

Figure 1. Molecular structures of the trinuclear $[\mathrm{LCoGdCoL}]^+$ entity **1**: (a) side view; (b) axial view. Color code: orange, Gd; green, Co; gray, C; blue, N; red, O. H ions are omitted for clarity. Red dashed lines denote the local anisotropy axes on Co ions, and green and red arrows are local magnetic moments on the Co and Gd ions in one of the components of the ground-state Kramers doublet of the complex.

All complexes exhibit similar static magnetic properties, as shown in Figure 3 for **1**, Figure S3 in the Supporting Information for **2**, and Figure S4 in the Supporting Information for **3**, respectively. The $\chi(T)-T$ plots show a sharp maximum, approximately at the same position, testifying about ferromagnetic interaction between metal ions of similar strength for all three compounds. By contrast, the dynamical magnetic properties differ drastically among the complexes. At zero direct-current (dc) field, frequency-dependent out-of-phase alternating-current (ac) susceptibility $\chi''(\omega)$ was detected for **1**−**3** in the frequency range from 1 to 1500 Hz, pointing to a slow relaxation of magnetization.[27] The SMM behavior in these complexes was further confirmed by measurements of magnetization hysteresis loops performed on single microcrystals (Figures S5 and S6 in the Supporting Information). These measurements have shown a more pronounced SMM behavior in **1**, which shows a coercive field of 8860 Oe at T = 0.3 K and a field-sweep rate as low as 0.002 T/s. Complex **2** shows a comparable coercive field, 7330 Oe, for a significantly higher field-sweep rate of 0.14 T/s, while complex **3** shows an even smaller coercive field. The relaxation times extracted from $\chi''(\omega)$ have shown an activated temperature behavior with a larger activation barrier for **1**, $U_{\mathrm{eff}} = 21.3$ K, than for **2**, $U_{\mathrm{eff}} = 14.5$ K, at zero dc field. Compared at equal temperatures, the relaxation times are longer in **1** (Figures S5 and S6 in the Supporting Information). A higher SMM performance of **1** compared to **2** and **3** seems surprising because the anisotropy comes only from $\mathrm{Co^{II}}$ ions in the former complex, while it is contributed also by the Ln ions in **2** and **3**. In order to gain further insight into this problem, we have performed ab initio calculations on complexes **1**−**3**.

EXPERIMENTAL AND COMPUTATIONAL DETAILS

The magnetic hysteresis loops have been measured on single crystals of **1**−**3** using a micro-SQUID technique.[30] The field was aligned with the easy axis of magnetization using a transverse field method.[31]

Ab initio calculations of mononuclear fragments have been done with the *MOLCAS 7.6* package.[32] All magnetic centers in **1**−**3** have been computed, using the crystallographic structure of the molecule. The neighboring magnetic centers were computationally described by the closest diamagnetic analogue: cobalt was substituted by zinc, while gadolinium, terbium, and dysprosium were substituted by La. For example, the fragment Co1 in **1** was actually a Co−La−Zn complex with the crystallographic position of all atoms. Basis sets describing all atoms were taken from the ANO-RCC[33] basis set library, available in the *MOLCAS* package.[32] Contractions of the employed basis sets are shown in the Supporting Information. The active space of the Complete Active Space Self-Consistent-Field (CASSCF) method[34] for cobalt fragments included seven electrons spanning the five 3d orbitals. Another set of five 3d orbitals was added to account for the double-shell effect.[35] For lanthanide fragments, the active space included the electrons from the last shell spanning seven 4f orbitals. For lanthanide fragments, we computed in a state-average calculation all roots arising from the considered active space. The dynamical correlation was added only to the two Co sites of **1** (Table 1) by means of the CASPT2 approach.[36,37] It was performed on the state-average CASSCF wave function on all states arising from the ligand field (10 quartet and 40 doublet spin states). The following shifts were employed to ensure feasibility and lack of intruder state problems: IMAG 0.1, IPEA- standard (0.25), and AFRE 0.1. Because of the fact that the dynamical correlation did not significantly change the results, CASPT2 was not further performed for the $\mathrm{Co^{2+}}$ sites of **2** and **3**. For lanthanide fragments, the dynamical correlation was not considered. The obtained spin terms in the CASSCF calculations were further mixed by the spin−orbit coupling within the Restricted Active Space State Interaction (RASSI) approach.[38] For lanthanide fragments, only a limited number of CASSCF states could possibly be mixed by spin−orbit coupling because of the hardware limitations. The obtained spin−orbit multiplets and ab initio computed matrix elements of the angular momentum were further used by the *SINGLE_ANISO* module[32] to compute the *g* tensors and local magnetic properties.[39] Thus, the magnetic properties of the individual metal ions have been treated by a parameter-free ab initio approach, in which the spin−orbit interaction is taken into account in a nonperturbative way.

Table 1. Energies ($\mathrm{cm^{-1}}$) of Low-Lying Quartet States[a] on Co1 and Co2 Fragments in 1; Notice the Large Separation of the Ground-State Term ^{4}E from the Excited-State Term$^4\mathrm{A_1}$

Co1		Co2	
CASSCF	CASPT2	CASSCF	CASPT2
0.0	0.0	0.0	0.0
49.6	57.3	120.0	120.6
3410.2	3395.9	3551.7	3535.0
7868.4	7772.2	8384.1	8311.9
8168.0	7999.3	8417.1	8330.4
8959.2	8807.5	9364.9	9264.4

[a] Only the lowest six spin quartet terms are shown here. All quartet (10) and all doublet (40) spin states were further mixed by the spin−orbit coupling in RASSI.

The magnetic coupling between Co−Ln and Co−Co metal pairs in **1**−**3** was further treated within the Lines model,[40] using the ab initio obtained energies and wave functions of the corresponding metal fragments. In this model, the isotropic exchange interaction between different spin terms of a given pair of metal fragments, which would arise in the absence of spin−orbit coupling on metal sites, is modeled by a single-parameter Heisenberg exchange Hamiltonian. Diagonalizing the matrix of this Hamiltonian written on the basis of spin−orbit multiplets of mononuclear metal fragments gives solutions corresponding to anisotropic exchange interactions between Kramers doublets of a given metal pair. This means that the obtained solutions are equivalent with the solutions of an anisotropic exchange Hamiltonian written in terms of pseudospins $\tilde{S} = {}^1/_2$ of Kramers doublets of two metal sites, generally described by nine exchange parameters. The main advantage of the employed Lines model is the use of only one single parameter (J) to simulate the anisotropic exchange coupling for each pair of metal fragments. The essential feature of this model is that it becomes exact in the limit of two fully isotropic metal ions and of two Ising metal ions (when both ions are strongly axial, e.g., characterized by one single direction of magnetization in the case of Kramers ions) or in the case of one isotropic and one Ising metal ion. In the present case, given the strong axiality of Co, Dy, and Tb ions in the investigated Co−Ln−Co complexes (vide infra), the Lines model is fully adequate. The simulations of the exchange spectrum have been done with a specially designed routine *POLY_ANISO*, which was interfaced with the *SINGLE_ANISO* program treating individual metal fragments. The obtained exchange spectrum and the corresponding wave functions of the polynuclear complex have been used for calculation of the temperature- and field-dependent magnetic properties of the polynuclear complex with the same routine *POLY_ANISO*. The exchange coupling constants $J_{\mathrm{Ln-Co}}$ and $J_{\mathrm{Co-Co}}$ are the only fitting parameters of the employed computational approach. The intermolecular interaction was considered in the mean field and described by one parameter (zJ). These parameters were extracted by a comparison of the experimental and calculated magnetisms. This computational methodology has been successfully applied for investigation of the magnetic properties of other mixed complexes containing transition-metal and Ln ions.[41,42]

RESULTS AND DISCUSSION

The fragment ab initio calculations for gadolinium, terbium, dysprosium, and all Co sites in **1**−**3** have been performed as described above (Tables 1−3 and S1 and S2 for **1**, S3 and S4 for **2**, and S5 and S6 for **3** in the Supporting Information). The

Table 2. Energies ($\mathrm{cm^{-1}}$) of the Low-Lying Kramers Doublets Arising from the Spin−Orbit Coupling on the Lowest ^{4}E and $^4\mathrm{A_1}$ Spin States[a]

Co1		Co2	
CASSCF/RASSI	CASPT2/RASSI	CASSCF/RASSI	CASPT2/RASSI
0.0	0.0	0.0	0.0
248.7	245.8	242.2	239.9
536.5	533.4	549.1	545.3
852.0	846.4	856.1	850.2
3771.6	3748.2	3880.8	3859.2
3847.4	3825.0	3954.8	3933.8

[a] The weight of the ^{4}E term in the four low-lying Kramers doublets is more than 99%, which confirms the first-order spin−orbit coupling.

Table 3. Main Values of the g Tensor in the Ground-State Kramers Doublets and Their Unquenched Orbital Moments (μ_B)

Co1		Co2	
CASSCF/RASSI	CASPT2/RASSI	CASSCF/RASSI	CASPT2/RASSI
g_x = 0.4197	g_x = 0.4085	g_x = 0.4066	g_x= 0.3974
g_y = 0.4233	g_y = 0.4120	g_y = 0.4155	g_y = 0.4059
g_z = 9.2928	g_z = 9.2817	g_z = 9.2570	g_z = 9.2464
unquenched orbital moment $\langle L_z \rangle$ in the ground-state doublet (μ_B)			
1.668	1.662	1.649	1.643

directions of the main anisotropy axes on metal ions (except for Gd, which is isotropic) are shown in Figures 1 and S1 and S2 in the Supporting Information by dashed lines. As expected from the structures of the compounds, they are almost perfectly aligned along the Co−Ln−Co axis. An exception is the local anisotropy axis on the dysprosium in **3**, which makes an angle of 14.2° with the direction Dy−Co1 and an angle of 15.1° with the direction Dy−Co2 (Figure S2 in the Supporting Information).

Unquenched Orbital Moments on Cobalt(II): beyond the Textbook Paradigm. The pseudotrigonal symmetry of the cobalt(II) environment makes the lowest two-spin quartets almost degenerate (Table 1), i.e., corresponding to the ^{4}E term of the C_3 group. The latter, being magnetic, will involve spin−orbit coupling already in the first order of the perturbation theory,[43] resulting, in particular, in large separations between low-lying Kramers doublets, which thus do not resemble the conventional zero-field splitting in cobalt(II) complexes.[44] Another consequence of the first-order spin−orbit coupling in these fragments is the large values of the g factors along the main anisotropy axis (g_z in Table 3), which are due to large unquenched orbital moments in this direction, $\langle L_z \rangle$. The latter have values larger than 1.5 μ_B (Table 3) that cannot be explained as originating solely from (split) octahedral ground-state term T_{1g},[59] a model used in almost all ligand-field treatments of cobalt(II) complexes.[43−50] Below we analyze in detail the reasons for the failure of this model in the present case.

In the case of an octahedral environment, the orbital momentum operator corresponding to the ground-state orbital triplet (T_{1g}) is proportional to the orbital momentum operator of a conventional atomic triplet term (P),[43,45] $\hat{L}(T_{1g}) = -A\hat{L}(P)$, with the proportionality coefficient $A = k_{orb}\ (3/2 - c_P{}^2)/(1 + c_P{}^2)$. Here k_{orb} is the orbital reduction factor, and c_P is the coefficient of an admixture of the $^4T_{1g}(P)$ to $^4T_{1g}(F)$ [^{4}F and ^{4}P are ground- and excited-state atomic terms of cobalt(II)] in the wave function of the ground-state triplet $^4T_{1g}$ of the octahedral cobalt(II) complex. In the case of a weak crystal field (compared to separation between ^{4}F and ^{4}P), c_P = 0, and $L(T_{1g}) = {}^3/_2 k_{orb}$ ($\approx {}^3/_2$ in the case of a weak metal−ligand covalency). In the opposite case, of strong ligand field, $c_P = {}^1/_2$ and $L(T_{1g}) = k_{orb}$ ($\approx$1 in the case of a weak covalency). The last is easily understood because the octahedral term in the strong ligand-field limit is given by a single electronic configuration (Scheme 1a) in which the orbital momentum comes from its noncompensation in the t_{2g} shell (middle t_{2g} orbital in Scheme 1a) $\langle L_z \rangle = k_{orb}[(2/3)^{1/2}\langle \mathbf{-2}| - 1/\sqrt{3}\langle \mathbf{+1}|]\ \hat{l}_z[(2/3)^{1/2}| - \mathbf{2}\rangle - 1/\sqrt{3}|\mathbf{+1}\rangle] = -k_{orb}$. Thus, in the case of octahedral geometry, the orbital momentum in the ground-state term $^4T_{1g}$ is found in the interval $k_{orb} \le L(^4T_{1g}) \le {}^3/_2 k_{orb}$, i.e., does not exceed $^3/_2$ even in the case of a weak covalency.

Scheme 1. Ground-State Strong-Field Electronic Configuration of Co^{2+} in O_h [Octahedral Environment (a)] and a C_3 Environment [Idealized Fragment of 1, Figure 1 (b)][a]

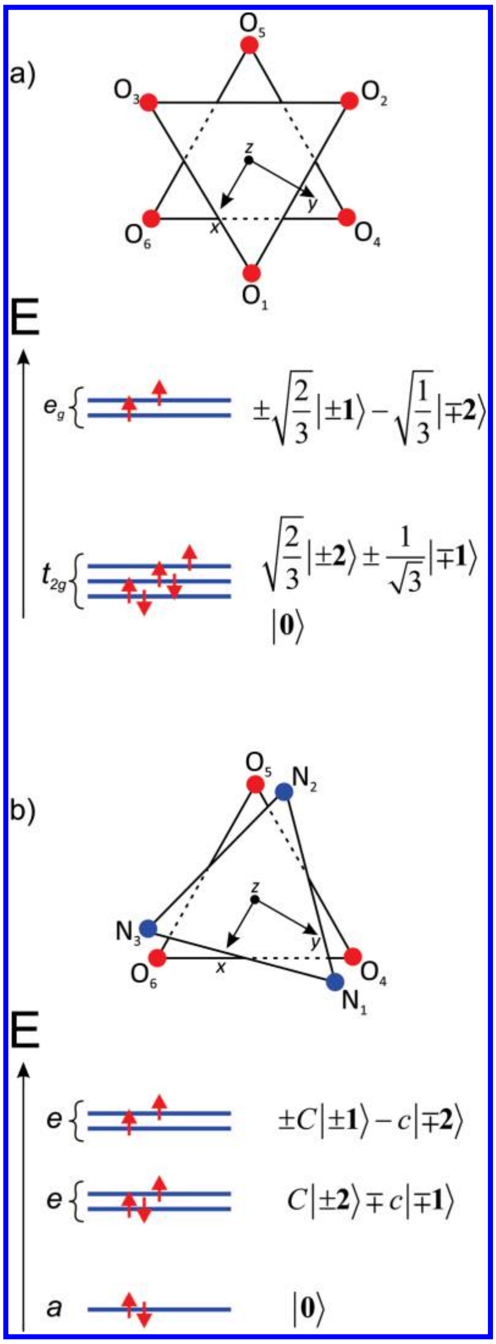

[a] In the latter case, $c < 1/\sqrt{3}$. Functions $|\pm m\rangle$ are complex 3d orbitals of Co^{2+}, with $|2,\pm m\rangle$ defined with respect to the trigonal quantization axis z (upper plots in parts a and b).

This situation does not change in the presence of weak low-symmetry components of the ligand field (e.g., due to small distortion of an octahedral geometry), so it is believed that the magnetism of the low-symmetry cobalt(II) complexes can be simulated by simply taking into account the splitting of the ground-state term $^4T_{1g}$.[43,45−47]

In the case of cobalt(II) fragments of **1**−**3**, the deviations of their geometry from an ideal octahedron cannot be considered small. Figure 1b shows (see also Scheme 1b) that the oxygen and nitrogen triangles (viewed from the trigonal axis) almost superimpose on each other, thus approaching trigonal-prismatic coordination geometry. In this case, the ground-state strong-field electronic configuration, corresponding to the molecular term ^{4}E (if we keep the trigonal symmetry), is characterized by a relatively large separation of the ground-state orbital a and first excited-state orbital doublet e (Scheme 1b). This large separation can be inferred from the excitation energy of the third spin quartet in Table 1, which corresponds to the electron transfer from the a orbital to the lowest e orbital in Scheme 1b. The ligand-field orbitals look similar to the corresponding orbitals for the octahedral coordination environment (Scheme 1a) but involve coefficients C and c ($C^2 + c^2 = 1$), which depend on the details of the geometry. In the case of an almost prismatic coordination, we have $c < 1/\sqrt{3}$ and the orbital momentum of the ^{4}E configuration in Scheme 1b, which comes entirely from one single orbital of the lowest e shell (the one that is doubly occupied), is $\langle L_z \rangle = k_{\mathrm{orb}}(C\langle \mathbf{-2}| + c\langle \mathbf{+1}|)\hat{l}_z(C|\mathbf{-2}\rangle + c|\mathbf{+1}\rangle) = -k_{\mathrm{orb}}(2 - 3c^2)$. This expression shows that the projection of the orbital momentum on the trigonal axis can exceed $^3/_2$ if the coefficient c is small enough and k_{orb} is close to unity. We note that c vanishes in the case of prismatic-like coordination with higher order of the main symmetry axis, in which case we can achieve the maximal value $\langle L_z \rangle = 2$ if k_{orb} is close to unity. Compared to this limiting value, the orbital momentum corresponding to Scheme 1b can be viewed as reduced by the factor $k = k_{\mathrm{orb}}(1 - 3c^2/2)$. Because the strong-field configuration in Scheme 1b can already provide $\langle L_z \rangle > {}^3/_2$, we may think that it should be preponderant in the wave function of the ground-state term ^{4}E. Indeed, the ab initio calculations show that the configuration in Scheme 1b enters the wave function of the ground-state spin quartet in Table 1 with a coefficient 0.96 for Co1 and 0.92 for Co2, which means that it is already a good approximation for the latter.

The obtained results allow for a straightforward derivation of the spin−orbit coupling operator for the ^{4}E term. The latter is characterized by two orbital configurations, the one shown in Scheme 1b and the other corresponding to repopulated orbital components of the lowest doublet e. At the same time, the a and the higher e orbital shells remain always populated like in Scheme 1b, i.e., correspond to zero total orbital moment of involved electrons in each of them. This means that these two shells will not contribute to the spin−orbit coupling, which thus can be written as

$$H_{\mathrm{SO}}(^4\mathrm{E}) = k_{\mathrm{orb}}\Sigma_{i=1}^{3}\zeta(\hat{s}_{ix}\hat{l}_{ix} + \hat{s}_{iy}\hat{l}_{iy} + \hat{s}_{iz}\hat{l}_{iz})$$

where the summation goes over the electrons of the lowest shell e. The nonzero contributions of the first two terms in the brackets involve matrix elements of $\hat{l}_{ix}$ and $\hat{l}_{iy}$ between the two orbitals of the lowest orbital doublet e, which are zero (this can be checked directly by using the corresponding orbital wave functions in Scheme 1b). Furthermore, in the remaining last term, only the electron from the unpaired orbital of the lowest shell e ($i = 1$) will contribute, whose orbital momentum is obviously $k_{\mathrm{orb}}\langle \hat{l}_{1z} \rangle = -\langle L_z \rangle = k \times 2$, the last equality corresponding to the configuration in Scheme 1b. Finally, taking into account that the matrix elements of $H_{\mathrm{SO}}(^4\mathrm{E})$ will be calculated on wave functions of $S = {}^3/_2$, corresponding to three ferromagnetically coupled electrons, we can replace $\hat{S}_{1z}$ by the z projection of the total spin,[49] $\hat{S}_{1z} = \hat{S}_z/2S$. Thus, the expression for the spin−orbit coupling for the ^{4}E terms has the following Ising form: $H_{\mathrm{SO}}(^4\mathrm{E}) = -k\lambda\hat{S}_z\hat{L}_z$, where $L_z = \pm 2$, as discussed above, and $\lambda = \zeta/2S = \zeta/3$ with $\zeta = 533$ cm^{-1} the spin−orbit coupling constant for cobalt(II).

The first-order spin−orbit coupling leads to the splitting of the ^{4}E term into four equidistant Kramers doublets. Choosing the orbital reduction constant $k = 0.801$, we obtain an almost perfect matching with the energies of the four Kramers doublets on two Co$^{\mathrm{II}}$ sites (Figure 2). For comparison, the reduction factor extracted from $\langle L_z \rangle = k \times 2$, gives $k = 0.829$, very close to the previous estimate, which proves once again that the configuration in Scheme 1b is a good approximation for the ground-state term. The ground-state Kramers doublet derived solely from this configuration is obtained perfectly axial, i.e., having $g_x = g_y = 0$. This is evident because the two wave functions of the ground-state Kramers doublet are $|S_z = -{}^3/_2, L_z = 2\rangle$ and $|S_z = -{}^3/_2, L_z = -2\rangle$, for which the matrix elements of transversal magnetic moments ($\hat{\mu}_x$ and $\hat{\mu}_y$) are zero. In the real cobalt(II) fragment, because of a small departure from C_3 symmetry (which causes the splitting of the ^{4}E term; Table 1) and a weak admixture of other electronic configurations (via interelectronic interaction within the 3d^7 shell of Co$^{\mathrm{II}}$), there appear small transversal components of the g tensor on Co$^{\mathrm{II}}$ (Tables 3 and S2, S4, and S6 in the Supporting Information). The single determinant character of the ground-state term ^{4}E (Scheme 1b) is the ultimate reason why g_x and g_y are unusually small, much smaller than those in most cobalt(II) complexes,[44] a fact having a crucial effect on the SMM properties of **1**−**3**, as emphasized below. Although the magnetic anisotropy in the ground-state Kramers doublets of the Co ions is obtained as highly axial, $g_{x,y}/g_z = 0.02$−0.04, it is not sufficient to block individual Co ions.

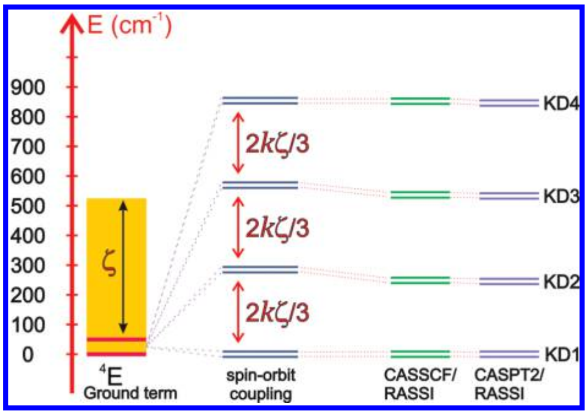

Figure 2. Effect of the first-order spin−orbit coupling on the ground-state term ^{4}E of the Co1 fragment in **1**. Three sets of levels show the results of the ligand field and ab initio calculations.

Blocking Barrier in Co−Gd−Co. In complex **1**, the whole anisotropy comes from Co ions,[51] while the magnetic blocking emerges as a common effect of this anisotropy and the exchange interaction in the complex. The latter has been treated within the Lines model,[40] in which an effective isotropic exchange Hamiltonian for $S = {}^3/_2$ on cobalt and $S = {}^7/_2$ on gadolinium

$$\hat{H}_{\mathrm{exch}} = J_1\hat{S}_{\mathrm{Gd}}\cdot(\hat{S}_{\mathrm{Co1}} + \hat{S}_{\mathrm{Co2}}) + J_2\hat{S}_{\mathrm{Co1}}\cdot\hat{S}_{\mathrm{Co2}} \qquad (1)$$

is projected on the basis of ab initio wave functions corresponding to the ground-state Kramers doublets on Co sites and the ground-state $S = {}^{7}/_{2}$ manifold on Gd sites.[41,42] The obtained exchange states and the local excitations on the metal sites above this exchange spectrum have been used for the simulation of $\chi(T)\ T$ and $M(H)$ of **1**, from which the exchange parameters J_1 and J_2 were derived (Figure 3). The obtained close values of these parameters is not surprising because the two Co ions are separated by a twice larger distance than Co and Gd, while at comparable distances, the Co−Co exchange is expected to be 1 order of magnitude larger. The spectrum of the lowest spin−orbit exchange multiplets of the complex, corresponding to the fitted exchange parameters, is shown in Figure 4. It consists of 32 exchange states, grouped in 16 Kramers doublets, which appear from two Kramers doublet components of each Co site and eight spin functions of a $S = {}^{7}/_{2}$ multiplet on a Gd site ($2 \times 2 \times 8 = 32$).

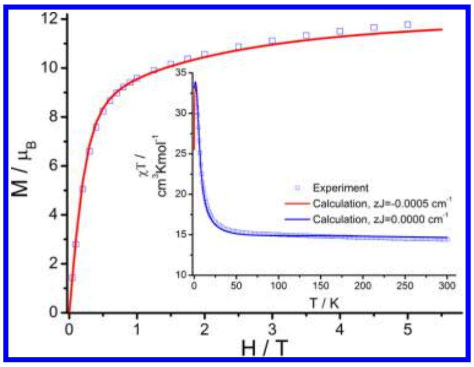

Figure 3. Magnetization (M) versus applied magnetic field (H) for **1**. Inset: variable-temperature molar magnetic susceptibility (χ) for **1**. Squares: measured data. Lines: ab initio based simulations with the exchange parameters $J_1 = 0.9$ cm^{-1}, $J_2 = 0.5$ cm^{-1}, and $zJ = -0.0005$ cm^{-1} for two values of the intermolecular interaction parameter zJ (see the text for details).

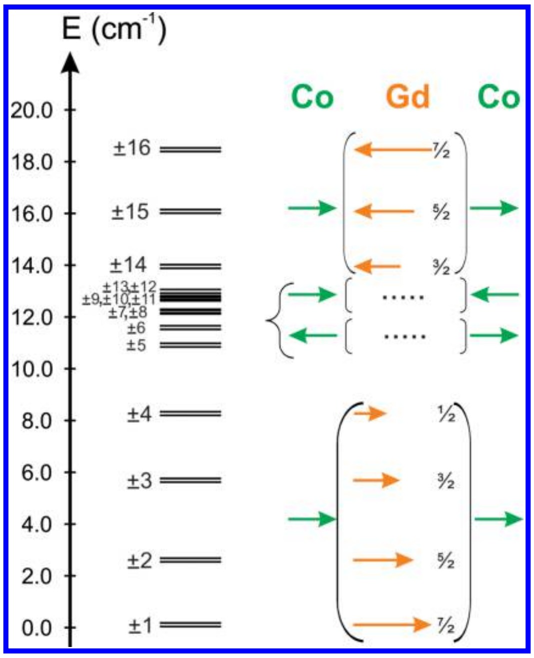

Figure 4. Exchange spectrum in **1**. The exchange Kramers doublets (left-hand side) and the internal magnetic structure of the corresponding states (right-hand side).

To understand the structure of the obtained exchange spectrum, one should remember that the exchange interaction between perfectly axial magnetic ions, for which the transversal g factors are exactly zero, is described by a (noncollinear) Ising model for the projections of pseudospin components on the local anisotropy axis of the metal ions (the Kramers doublets on Co sites are described by pseudospins $\tilde{S} = {}^{1}/_{2}$). An exchange spectrum of this type has been recently found in Dy_3 triangles.[52] Similarly, the exchange interaction between a perfectly axial Kramers doublet and an isotropic spin reduces to a (collinear) Ising model between the projection of pseudospin on the corresponding anisotropy axis and the projection of the isotropic spin in the same direction. Then, if Co ions were perfectly axial, the exchange interaction between all three metal ions in **1** would have been of a net Ising type. However, as the ab initio calculations have shown, the magnetic anisotropy on the Co sites is strongly but not perfectly axial, which means that the exchange spectrum will not be entirely of the Ising type. Accordingly, the exchange spectrum in Figure 4 shows that only the lowest four and the highest three exchange doublets are equidistant, as for an Ising exchange interaction. The structure of these exchange states (right-hand side of Figure 4) shows indeed that the ions are characterized by definite projections of magnetic moments as for an Ising state. A comparison of the obtained exchange energies and the energies obtained in the case when the μ_x and μ_y components of the magnetic moment of the ground-state Kramers doublet on Co^{II} ions were set to zero (to make Co^{II} ions perfectly axial) are given in Table S7 in the Supporting Information. Analysis of energies in Table S7 in the Supporting Information confirms that the departure from a pure Ising interaction in **1** is not significant.

Thus, the two Co ions have maximal projections of magnetic moments on their local anisotropy axes (they are almost parallel to each other), while the Gd ion is characterized by a definite projection of spin (and magnetic moment) in the same direction. The ground-state exchange Kramers doublet corresponds to a maximal projection $M = {}^{7}/_{2}$ of gadolinium spin in the direction of cobalt momenta, resulting in the maximal magnetic moment of the complex (Figure 1). The excited-state exchange Kramers doublets, 2−4 (Figure 4), correspond to $M = {}^{5}/_{2}$, ${}^{3}/_{2}$, and ${}^{1}/_{2}$, respectively, at the unchanged directions of local magnetizations on Co sites. This gradual decrease of M with increasing energy of the exchange doublet resembles much the structure of the blocking barrier in the conventional SMMs for complexes in the strong exchange limit, like Mn_{12}ac.[1,2] The main difference is that in the latter the splitting of the ground-state spin manifold follows a parabolic dependence, $E_M = |D|M^2$, while in the case of **1**, it is almost equidistant. On the other hand, the states in the middle of the exchange spectrum (5−13 in Figure 4) are not of the pure Ising type but are rather mixtures of them.

In order to determine the structure of the barrier of blocking of magnetization on the basis of calculated exchange states, we must assess the most efficient relaxation paths from a state with maximal magnetization in the ground-state exchange doublet (Figure 1) to the time-reversed state, with reversed magnetization (Figure 5). The two basic relaxation mechanisms are due to QTM and the spin−phonon transitions.[2] The former consists of (i) direct tunneling between the two components of

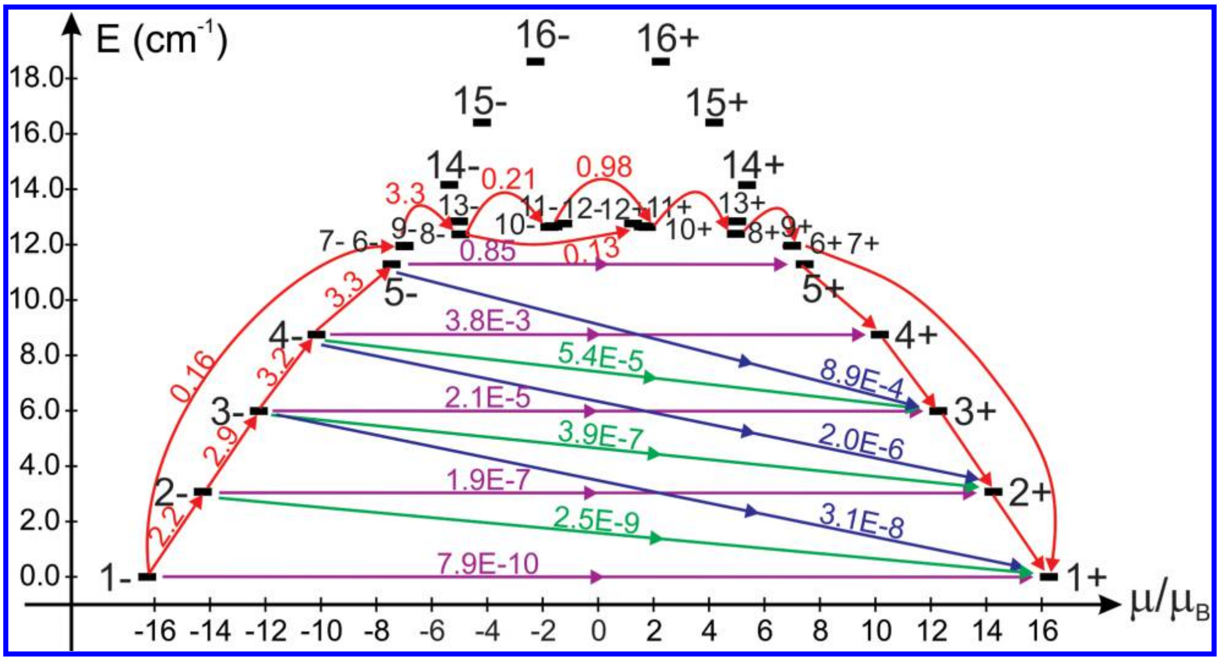

Figure 5. Magnetization blocking barrier in **1**. The exchange states are arranged according to the values of their magnetic moments. The arrows show the connected exchange states, and the numbers at each of them stand for the corresponding matrix element of the transversal magnetic moment (see the text for details).

a given doublet and of (ii) indirect tunneling via excited-state exchange states, induced by a Zeeman interaction with a transverse magnetic field (externally applied or present in the crystal).[53,54] The direct QTM arises in Kramers complexes like **1** and **3** because of first-order Zeeman splitting of the doublet states, induced by a transversal magnetic field, which is proportional to the matrix element of the transversal magnetic moment between the two doublet states. In non-Kramers complexes like **2**, this matrix element is exactly zero in virtue of Griffith's theorem,[43,55] while the direct QTM is due to an intrinsic tunneling gap (Δ_{tun}), present in such complexes without any applied field. On the other hand, the matrix elements of the spin−phonon coupling in axial complexes are defined in the commonly used "rotational approximation"[2] by the matrix elements of $\hat{S}_x$ and $\hat{S}_y$ for pure spin systems[53,54] and of $\hat{J}_x$ and $\hat{J}_y$ for Ln ions,[56,57] both of which are proportional to the matrix elements of transversal components of the magnetic moment. Thus, the matrix elements of transversal magnetic moments and the intrinsic tunneling gaps define the basic relaxation mechanisms in our complexes. Then the blocking barrier can be defined by the shortest paths, where these quantities are the largest.

Figure 5 shows the exchange states of **1** (Figure 4) arranged according to the values of their magnetic moments, which is maximal in the direction close to the trigonal axis of the complex, for each exchange doublet. The number at each arrow connecting two states is the root-mean-square value of matrix elements of magnetic moments (in μ_B) between the corresponding states, calculated on the ab initio wave functions of the complex. We can see that the magnetic moment matrix element for the ground-state exchange doublet is extremely small, so that no direct QTM can be expected. The largest matrix elements are obtained for the lowest states 1−4, corresponding to the gradual reversal of the Gd spin (Figure 4), and also between ±4 and ±5 and between +5 and −5, as indicated by red arrows in Figure 5. These arrows, connecting the nearest-neighbor states, delineate a barrier of reversal of magnetization, which resembles the one observed in SMMs characterized by pure spin, like $Mn_{12}ac$.[2] As an additional confirmation for this analogy, all other matrix elements involving these states are several orders of magnitude smaller. One can say, therefore, that this barrier is of a "pure-spin" type. There is also a second barrier in **1**, corresponding to the spin−phonon transition from the ground-state component −1 to the excited state −6, then the transition from −6 to −7, −8, and −10, and then to the time-reversed states in the opposite order. The corresponding barrier is delineated in Figure 5 by curved red arrows. At variance with the "pure-spin" barrier, it involves only mixed excited states (Figure 4). On the other hand, the magnetic moment matrix element connecting −6 and −7 with +6 and +7 directly is on the order of 10^{-3} μ_B, so that the corresponding tunneling transition between these states is less efficient. Note that there are no other appreciable magnetic moment matrix elements connecting the ground state −1 with other excited states besides those shown in Figure 5. Also there is no appreciable connection between the states forming the "pure-spin" barrier, notably −5 and +5, with the states of the "mixed" barrier. We note that the top of the latter, 12.6 cm^{-1}, compares well with U_{eff} = 21.3 K = 14.6 cm^{-1} extracted from the ac measurements.[27] The QTM in **1** is only of the indirect type, i.e., due to the Zeeman interaction with a transverse magnetic field.

Blocking Barrier in Co−Tb−Co. The exchange spectrum in **2** was calculated within the same Lines model, eq 1, where $\hat{S}_{\mathrm{Gd}}$ was replaced by $\hat{S}_{\mathrm{Tb}}$ = 3, projected on the basis of the ab initio states corresponding to the ground-state Kramers doublets on Co sites and the two lowest states on Tb. The latter form a doublet split by ca. 0.02 cm^{-1} (Table S3 in the Supporting Information). The obtained exchange states and the local excitations on the metal sites above this exchange spectrum have been used for the simulation of $\chi(T)\ T$ and $M(H)$ of **2**; parameters J_1 and J_2 were derived (Figure S3 in the Supporting Information). The spectrum of the lowest spin–orbit exchange multiplets of the complex, corresponding to the fitted exchange parameters, is shown in Figure 6a. It consists of eight exchange states that are all nondegenerate but can still be grouped into four Ising-like doublets, which derive from two Kramers doublet components of each Co site and two lowest states on a Tb site ($2 \times 2 \times 2 = 8$). The obtained exchange spectrum is almost of the Ising type, with the main deviation being the small energy separation between the doublets 2 and 3 in Figure 6a, which comes from the mixing of two Ising components corresponding to opposite directions of magnetizations on the Co sites (right-hand side of Figure 6a). At the same time, the ground-state doublet contains two Ising-like states with maximal possible magnetization (Figure S1 in the Supporting Information).

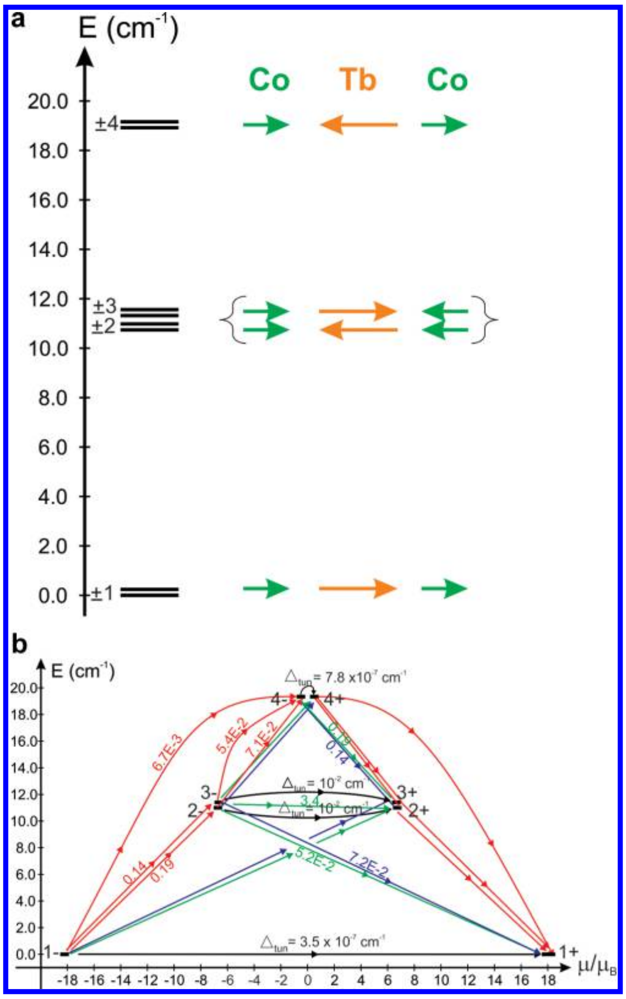

Figure 6. Exchange spectrum and magnetization blocking barrier in **2**: (a) exchange doublets (left-hand side) and the internal magnetic structure of the corresponding states (right-hand side); (b) exchange states arranged according to the values of their magnetic moments. The arrows show the connected exchange states, and the numbers at each of them stand for the corresponding matrix element of the transversal magnetic moment. The horizontal black arrows connect states split by an intrinsic tunneling gap (see the text for details).

Figure 6b shows the exchange states of **2** arranged according to the value of the maximal magnetic moment arising in each of the four doublets. Again, as in **1**, the direction of this magnetic moment is close to the trigonal axis of the complex. The spin–phonon relaxation path connecting −1 and −2 can either go via one single state, −2 or −3 (Orbach or Raman processes[45]) or involve an additional step of resonance tunneling between −2, +2 and −3, +3 (thermally activated tunneling mechanism[53]). The activation barrier extracted from ac measurements, U_{eff} = 14.5 K = 9.9 cm^{-1}, compares well with energies of the excited exchange states 2 and 3 (11.2 cm^{-1} in Table S8 in the Supporting Information). We should note that, according to the data in Figure 6b, the relaxation path between −2, −3 and +2, +3 should be efficient because, besides the intrinsic tunneling gaps in each of the doublets 2 and 3, there is a very large magnetic moment matrix element of ca 3 μ_B between the states −3, +2 and +3, −2, separated by only 0.03 cm^{-1} (Table S8 in the Supporting Information), which is expected to induce relatively large Zeeman splitting in the presence of a transverse magnetic field. This probably explains why the relaxation of magnetization in **2** does not change after application of a longitudinal dc field of 1000 Oe;[27] it is simply not sufficient to suppress the tunneling in the excited doublets 2 and 3. However, a dc field of 3000 Oe increases the activation barrier to U_{eff} = 20.9 K,[27] which can be explained as a result of suppression of tunneling dynamics within the doublets 2 and 3. Indeed, after this suppression, the path involving the next excited state 4 becomes operative because it is characterized by comparable magnetic moment matrix elements as the lowest path (Figure 6b). The two relaxation processes will take place concomitantly, while the value of the activation barrier extracted from ac measurements (20.9 K) falls between the excitation energies to the states 2, 3 and the state 4. The intrinsic tunneling gap for the lowest exchange doublet in **2** is on the order 10^{-7} cm^{-1} (Figure 6b).

Blocking Barrier in Co–Dy–Co. A similar treatment of the exchange interaction for complex **3** (with $\hat{S}_{\mathrm{Gd}}$ in eq 1 replaced by $\hat{S}_{\mathrm{Dy}} = {}^{5}/_{2}$ including the projection on the lowest Kramers doublets of the Co1, Dy, and Co2 sites (Table S6 in the Supporting Information), after the fitting of $\chi(T)\ T$ and $M(H)$ (Figure S4 in the Supporting Information) and extraction of J_1 and J_2 yield the spectrum of lowest exchange levels shown in Figure 7a. The four exchange Kramers doublets arise from the two components of the lowest Kramers doublets on the Co1, Co2, and Dy sites ($2 \times 2 \times 2 = 8$). The scheme of exchange states arranged according to the values of their magnetic moments (again, almost parallel to the common axis of the complex) gives a scheme in Figure 7b that is similar to the scheme in Figure 6b for **2**. Also, the values of the magnetic moment matrix elements are comparable in both schemes, thus implying common relaxation mechanisms in both complexes (the only difference is the relaxation within the doublets 2 and 3, which is driven by intrinsic tunneling gaps in **2** and is of Zeeman origin in **3**).

Finally, the above calculations explain why QTM is fast in **3**, relatively slow in **2**, and the slowest for **1**. Indeed, the jump of magnetization at H = 0 is large for dysprosium, small for terbium, and almost absent for gadolinium (parts c, b, and a, respectively, in Figure S6 in the Supporting Information). The height of these magnetization steps are proportional to the probability of transition between the two Zeeman components of the ground-state exchange doublet when the field is swept through the H = 0 point. According to Landau–Zener–

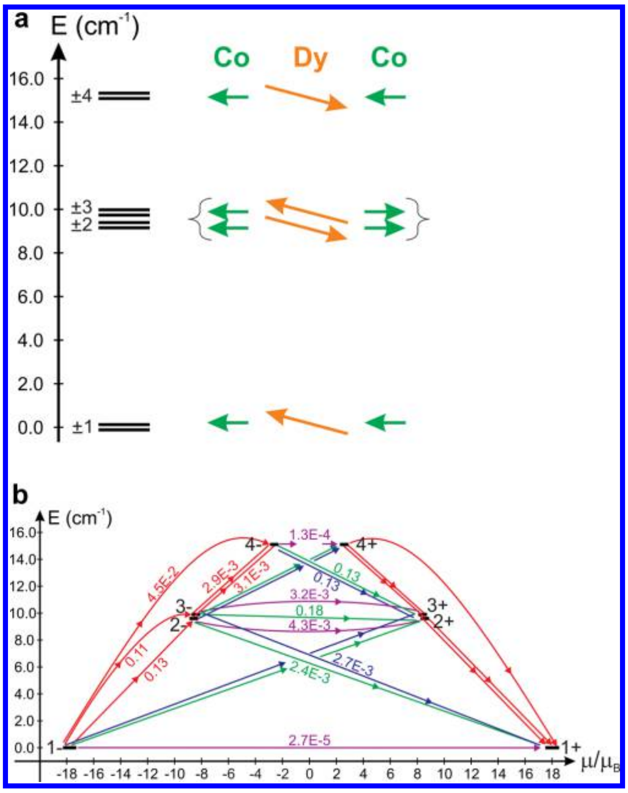

Figure 7. Exchange spectrum and magnetization blocking barrier in **3**: (a) exchange Kramers doublets (left-hand side) and the internal magnetic structure of the corresponding states (right-hand side); (b) exchange states arranged according to the values of their magnetic moments. The arrows show the connected exchange states, and the numbers at each of them stand for the corresponding matrix element of the transversal magnetic moment (see the text for details).

Stückelberg theory,[2] this probability depends on the tunneling splitting Δ_t, when it is relatively small, approximately as $\sim\Delta_t^2$.

Figure 8 shows the calculated Δ_t for the ground-state exchange doublet of the three complexes as a function of the transversal field. The intrinsic tunneling gap in **2** remains practically unchanged, which is a consequence of the absence of the linear Zeeman effect for transverse fields. By contrast, the latter is mainly responsible for the opening of the gap in **3**, which is the result of a nonnegligible transversal magnetic moment matrix element for the ground-state doublet (Figure 7b). On the other hand, this matrix element is negligible in **1**, where Δ_t is very small at moderate transverse fields and due to many intermediate states involved in both barriers (Figure 5). Figure 8 shows that, for typical values of internal fields (30−40 mT), Δ_t is smallest for **1** and largest for **3**, in agreement with what we infer from Figure S6 in the Supporting Information. We should note that QTM is further enhanced in **2** and **3** via hyperfine coupling on Tb and Dy ions, respectively,[58] while this effect is absent for Gd.

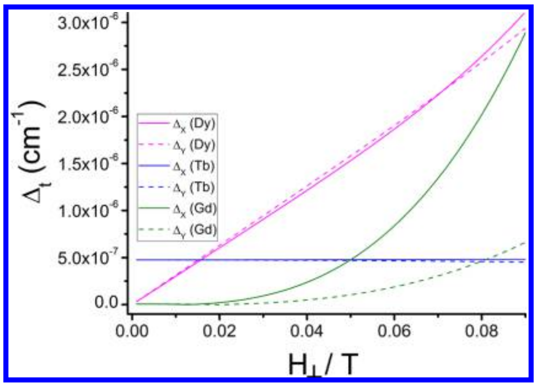

Figure 8. Tunneling splitting of the ground-state exchange doublet versus applied transversal magnetic field in **1**−**3**. x and y are the directions corresponding to the transversal g factors g_x and g_y, respectively, of the ground-state doublet of the complexes (Tables S7−S9 in the Supporting Information).

■ CONCLUSIONS

The fragment ab initio calculations showed that the Co^{II} sites in complexes **1**−**3** preserve large unquenched orbital momentum in the ground state (ca. 1.7 μ_B), leading through the first-order spin−orbit coupling, to unexpectedly strong uniaxial magnetic anisotropy, comparable to Ln ions (e.g., Dy^{3+}). Furthermore, it turns out that it is this anisotropy that makes all three compound SMMs.

Applying an originally developed ab initio based analysis of the magnetization blocking barriers in complexes **1**−**3**, we found qualitative differences between them, which explain the experimental findings. Namely, the much stronger suppression of QTM in **1** compared to **2** and **3** is due to qualitative differences in the structure of blocking barriers. The latter consists of several excited states in **1**, while it involves only one excited state in **2** and **3**. The reason for this is the higher (8-fold) degeneracy of the ground-state multiplet on the Gd site in **1** compared to the ground-state manifolds on the Ln sites in **2** and **3**, which are only 2-fold degenerate. This leads to a denser exchange spectrum in the former compound and, as a result, to multilevel blocking barriers. This conclusion seems to be general for other polynuclear complexes involving strongly anisotropic metal sites. It could well be that the right strategy for the design of efficient SMMs is to combine in one compound strongly anisotropic and completely isotropic metal ions with large angular momentum. Besides suppression of QTM, an efficient SMM should also possess a high barrier of reversal of magnetization, which at its turn is determined by the strength of exchange interactions between the ions. Both of these requirements are probably best met in mixed 4,5f−4,5d complexes.

■ ASSOCIATED CONTENT

Ⓢ Supporting Information

Magnetism of **2** and **3**, single-crystal hysteresis loops at low temperature, calculated energies and g tensors of individual metal sites, exchange interactions, and a comparison of the exchange energies. This material is available free of charge via the Internet at http://pubs.acs.org.

■ AUTHOR INFORMATION

Corresponding Author

*E-mail: Liviu.Chibotaru@chem.kuleuven.be.

Notes

The authors declare no competing financial interest.

■ ACKNOWLEDGMENTS

This work was supported by the European Union sixth framework program NMP3-CT-2005-515767 entitled “MAG-

MANet: Molecular Approach to Nanomagnets and Multifunctional Materials" and was partially supported by the ANR-PNANO project MolNanoSpin ANR-08-NANO-002 and the ERC Advanced Grant MolNanoSpin 226558. L.U. is postdoc FWO (Flemish Science Foundation) and acknowledges support by INPAC and Methusalem grants from KU Leuven.

REFERENCES

(1) Sessoli, R.; Gatteschi, D.; Caneschi, A.; Novak, M. A. *Nature* **1993**, *365*, 141.

(2) Gatteschi, D.; Sessoli, R.; Villain, J. *Molecular Nanomagnets*; Oxford University Press: Oxford, U.K., 2006.

(3) Gambardella, P.; Stepanow, S.; Dmitriev, A.; Honolka, J.; de Groot, F. M. F.; Lingenfelder, M.; Gupta, S. S.; Sarma, D. D.; Bencok, P.; Stanescu, S.; Clair, S.; Pons, S.; Lin, N.; Seitsonen, A. P.; Brune, H.; Barth, J. V.; Kern, K. *Nat. Mater.* **2009**, *8*, 189.

(4) Leuenberger, M. N.; Loss, D. *Nature* **2001**, *410*, 789.

(5) Bogani, L.; Wernsdorfer, W. *Nat. Mater.* **2008**, *7*, 179.

(6) Timco, G. A.; Carretta, S.; Troiani, F.; Tuna, F.; Pritchard, R. J.; Muryn, C. A.; McInnes, E. J. L.; Ghirri, A.; Candini, A.; Santini, P.; Amoretti, G.; Affronte, M.; Winpenny, R. E. P. *Nat. Nanotechnol.* **2009**, *4*, 173.

(7) Bencini, A.; Gatteschi, D. *EPR of Exchange-Coupled Systems*; Springer: Berlin, 1990.

(8) Gatteschi, D.; Sorace, L. *J. Solid State Chem.* **2001**, *159*, 253.

(9) (a) Waldmann, O. *Inorg. Chem.* **2007**, *46*, 10035. (b) Ruiz, E.; Cirera, J.; Cano, J.; Alvarez, S.; Loose, C.; Kortus, J. *Chem. Commun.* **2008**, *1*, 52.

(10) Neese, F.; Pantazis, D. A. *Faraday Discuss.* **2011**, *148*, 229.

(11) Neese, F.; Solomon, E. I. *Inorg. Chem.* **1998**, *37*, 6568.

(12) Villain, J.; Hartman-Boutron, F.; Sessoli, R.; Rettori, A. *Europhys. Lett.* **1994**, *27*, 159.

(13) Sessoli, R.; Powell, A. K. *Coord. Chem. Rev.* **2009**, *253*, 2328.

(14) Ishikawa, N.; Sugita, M.; Ishikawa, T.; Koshihara, S.; Kaizu, Y. *J. Phys. Chem. B* **2004**, *108*, 11265.

(15) AlDamen, M. A.; Cardona-Serra, S.; Clemente-Juan, J. M.; Coronado, E.; Gaita-Ariño, A.; Martí-Gastaldo, C.; Luis, F.; Montero, O. *Inorg. Chem.* **2009**, *48*, 3467.

(16) Harman, W. H.; Harris, T. D.; Freedman, D. E.; Fong, H.; Chang, A.; Rinehart, J. D.; Ozarowski, A.; Sougrati, M. T.; Grandjean, F.; Long, G. J.; Long, J. R.; Chang, C. J. *J. Am. Chem. Soc.* **2010**, *132*, 18115.

(17) Ungur, L.; Chibotaru, L. F. *Phys. Chem. Chem. Phys.* **2011**, *13*, 20086.

(18) Lin, P.-H.; Burchell, T. J.; Ungur, L.; Chibotaru, L. F.; Wernsdorfer, W.; Murugesu, M. *Angew. Chem., Int. Ed.* **2009**, *48*, 9489.

(19) Blagg, R. J.; Muryn, C. A.; McInnes, E. J. L.; Tuna, F.; Winpenny, R. E. P. *Angew. Chem., Int. Ed.* **2011**, *50*, 6530.

(20) Hewitt, I. J.; Tang, J.; Madhu, N. T.; Anson, C. E.; Lan, Y.; Luzon, J.; Etienne, M.; Sessoli, R.; Powell, A. K. *Angew. Chem., Int. Ed.* **2010**, *49*, 6352.

(21) Guo, Y.-N.; Xu, G.-F.; Wernsdorfer, W.; Ungur, L.; Guo, Y.; Tang, J.; Zhang, H.-J.; Chibotaru, L. F.; Powell, A. K. *J. Am. Chem. Soc.* **2011**, *133*, 11948.

(22) Rinehart, J. D.; Fang, M.; Evans, W. J.; Long, J. R. *Nat. Chem.* **2011**, *3*, 538.

(23) Rinehart, J. D.; Fang, M.; Evans, W. J.; Long, J. R. *J. Am. Chem. Soc.* **2011**, *133*, 14236.

(24) Costes, J.-P.; Dahan, F.; Wernsdorfer, W. *Inorg. Chem.* **2006**, *45*, 5.

(25) Li, M.; Lan, Y.; Ako, A. M.; Wernsdorfer, W.; Anson, C. E.; Buth, G.; Powell, A. K.; Wang, Z.; Gao, S. *Inorg. Chem.* **2010**, *49*, 11587.

(26) Kajiwara, T.; Nakano, M.; Takahashi, K.; Takaishi, S.; Yamashita, M. *Chem.—Eur. J.* **2011**, *17*, 196.

(27) Yamaguchi, T.; Costes, J. -P.; Kishima, Y.; Kojima, M.; Sunatsuki, Y.; Bréfuel, N.; Tuchagues, J. -P.; Vendier, L.; Wernsdorfer, W. *Inorg. Chem.* **2010**, *49*, 9125.

(28) Chandrasekhar, V.; Pandian, B. M.; Azhakar, R.; Vittal, J. J.; Clérac, R. *Inorg. Chem.* **2007**, *46*, 5140.

(29) Chandrasekhar, V.; Pandian, B. M.; Vittal, J. J.; Clérac, R. *Inorg. Chem.* **2009**, *48*, 1148.

(30) Wernsdorfer, W. *Adv. Chem. Phys.* **2001**, *118*, 99.

(31) Wernsdorfer, W.; Chakov, N. E.; Christou, G. *Phys. Rev. B* **2004**, *70*, 132413.

(32) Aquilante, F.; De Vico, L.; Ferré, N.; Ghigo, G.; Malmqvist, P.-Å.; Neogrády, P.; Pedersen, T. B.; Pitoňák, M.; Reiher, M.; Roos, B. O.; Serrano-Andrés, L.; Urban, M.; Veryazov, V.; Lindh, R. *J. Comput. Chem.* **2010**, *31*, 224.

(33) Roos, B. O.; Lindh, R.; Malmqvist, P.-Å.; Veryazov, V.; Widmark, P.-O. *J. Phys. Chem. A* **2005**, *109*, 6575.

(34) Roos, B. O.; Malmqvist, P.-Å. *Phys. Chem. Chem. Phys.* **2004**, *6*, 2919.

(35) Andersson, K.; Roos, B. O. *Chem. Phys. Lett.* **1992**, *191*, 507.

(36) Andersson, K.; Malmqvist, P.-Å.; Roos, B. O.; Sadlej, A. J.; Wolinski, K. *J. Phys. Chem.* **1990**, *94*, 5483.

(37) Andersson, K.; Malmqvist, P.-Å.; Roos, B. O. *J. Chem. Phys.* **1992**, *96*, 1218.

(38) Malmqvist, P.-Å.; Roos, B. O.; Schimmelpfennig, B. *Chem. Phys. Lett.* **2002**, *357*, 230.

(39) Chibotaru, L. F.; Ungur, L. *J. Chem. Phys.* **2012**, *137*, 064112.

(40) Lines, M. E. *J. Chem. Phys.* **1971**, *55*, 2977.

(41) Mondal, K. C.; Sundt, A.; Lan, Y.; Kostakis, G. E.; Waldmann, O.; Ungur, L.; Chibotaru, L. F.; Anson, C. E.; Powell, A. K. *Angew. Chem., Int. Ed.* **2012**, *51*, 7550.

(42) Chibotaru, L. F.; Ungur, L.; Aronica, C.; Elmoll, H.; Pilet, G.; Luneau, D. *J. Am. Chem. Soc.* **2008**, *130*, 12445.

(43) Griffith, J. S. *The Theory of Transition-Metal Ions*; Cambridge University Press: Cambridge, U.K., 1971.

(44) Boča, R. *Coord. Chem. Rev.* **2004**, *248*, 757.

(45) Abragam, A.; Bleaney, B. *Electron Paramagnetic Resonance of Transition Ions*; Clarendon Press: Oxford, U.K., 1970.

(46) Kahn, O. *Molecular Magnetism*; VCH: Weinheim, Germany, 1993.

(47) Boča, R. *Theoretical Foundations of Molecular Magnetism*; Elsevier: Amsterdam, The Netherlands, 1999.

(48) Herrera, J. M.; Bleuzen, A.; Dromzée, Y.; Julve, M.; Lloret, F.; Verdaguer, M. *Inorg. Chem.* **2003**, *42*, 7052.

(49) Van den Heuvel, W.; Chibotaru, L. F. *Inorg. Chem.* **2009**, *48*, 7557.

(50) Landau, L. D.; Lifshitz, E. M. *Quantum Mechanics*, 2nd ed.; Pergamon: Oxford, U.K., 1975.

(51) Murrie, M. *Chem. Soc. Rev.* **2010**, *39*, 1986.

(52) Chibotaru, L. F.; Ungur, L.; Soncini, A. *Angew. Chem., Int. Ed.* **2008**, *47*, 4126.

(53) Garanin, D. A.; Chudnovsky, E. M. *Phys. Rev. B* **1997**, *56*, 11102.

(54) Leuenberger, M. N.; Loss, D. *Phys. Rev. B* **2000**, *61*, 1286.

(55) Griffith, J. S. *Phys. Rev.* **1963**, *132*, 316.

(56) Dohm, V.; Fulde, P. *Z. Physik. B* **1975**, *21*, 369.

(57) Luis, F.; Martínez-Pérez, M. J.; Montero, O.; Coronado, E.; Cardona-Serra, S.; Martí-Gastaldo, C.; Clemente-Juan, J. M.; Sesé, J.; Drung, D.; Schurig, T. *Phys. Rev. B* **2010**, *82*, 060403(R).

(58) Ishikawa, N.; Sugita, M.; Wernsdorfer, W. *Angew. Chem., Int. Ed.* **2005**, *44*, 2931.

(59) We are grateful to the reviewers for pointing this out.